J Solid State Eletrochem (2004) 8: 174–181
DOI 10.1007/s10008-003-0447-z

ORIGINAL PAPER

K. Nishikawa · M. Ota · S. Izuo · Y. Fukunaka
E. Kusaka · R. Ishii · J. R. Selman

Transient natural convection induced by electrodeposition of Li^+ ions onto a lithium metal vertical cathode in propylene carbonate

Received: 18 March 2003 / Accepted: 11 August 2003 / Published online: 7 October 2003

Abstract Transient natural convection caused by Li^+ electrodeposition at constant current along a vertical Li metal cathode immersed in a 0.5 M $LiClO_4$–PC (propylene carbonate) electrolyte was compared with that by Cu^{2+} ion electrodeposition in aqueous $CuSO_4$ solution. The concentration profile of the Li^+ ions was measured in situ by holographic interferometry. The interference fringes start to shift with time at a higher current density. The concentration boundary layer thickness for Li^+ ions was successfully determined. With the progress of electrodeposition, the density difference between the electrolyte at the cathode surface and the bulk electrolyte increased to induce upward natural convection of the electrolyte. The electrolyte velocity was measured by monitoring the movement of tracer particles. The measured transient behavior of the ionic mass and momentum transfer rates normalized with respect to the steady-state value was numerically analyzed. Transient natural convection along a vertical cathode due to Li metal electrodeposition can be reasonably explained by boundary layer theory, similar to the case of Cu electrodeposition in aqueous $CuSO_4$ solution.

Keywords Electrodeposition · Holographic interferometry · Ionic mass transfer · Lithium · Transient natural convection

K. Nishikawa · M. Ota · S. Izuo · Y. Fukunaka (✉)
E. Kusaka · R. Ishii
Department of Energy Science and Technology,
Graduate School of Energy Science,
Kyoto University,
Sakyo-ku, Kyoto, Japan
E-mail: fukunaka@energy.kyoto-u.ac.jp
Tel.: +81-75-7535415
Fax: +81-75-7534719

J. R. Selman
Center for Electrochemical Science and Engineering,
Illinois Institute of Technology,
Chicago, IL 60616, USA

Introduction

Natural convective flow develops along the surface of a vertical plane electrode installed in an unstirred electrolyte when current is spontaneously passed. It interacts with the ionic mass transfer rate and the resultant current density distribution along the vertical direction. Moreover, it starts to couple with the morphological variation of the electrodeposited metal. Most of the theoretical and experimental research thus far has dealt only with steady laminar natural convective flow. The electrodeposition of Cu^{2+} ions in aqueous $CuSO_4$ solution has been used to understand the interaction between electrochemical and transport phenomena since the 1940's work of Wagner [1] and Brenner [2]. The analysis of transient natural convection is also practically important, e.g. for designing the operational scheduling of unsteady-state industrial electrolysis such as periodic reverse current electrolysis. It is also indispensable to interpret certain data measured in cyclic voltammetry, when a vertically oriented plate or foil electrode is employed.

Natural convection in a Li deposition system: why?

Lithium batteries, like most high-energy-density or high-power-density batteries, are designed such that the electrolyte layer between the electrodes is very thin and therefore presents minimal ohmic resistance. Often the electrolyte is contained within a microporous membrane or diaphragm, which prevents electronic contact (shorting) between the electrodes due to accidental distortion, etc. Therefore, natural convection in lithium batteries is practically excluded. However, the phenomenological understanding of lithium metal electrodeposition and dissolution, and especially the reversibility of the process, can be studied advantageously in a cell that features natural convection. In the literature, there are many reports about lithium electrodeposition from surface chemistry [3, 4, 5, 6, 7]. The important practical

aspect of dendrite formation on lithium metal has been investigated and interpreted on the basis of a passivative layer concept [8, 9]. However, the connection of these phenomena with ionic mass transfer in the non-aqueous electrolyte has not frequently been considered. Transient natural convection is induced by the electrodeposition of Li^+ ions onto a Li metal cathode also in organic electrolyte solutions, as long as the densification coefficient is appreciable, since the solutions are typically of molar strength. There is good reason to assume that the ionic mass transfer rate of Li^+ ions is coupled with the dendrite growth at a Li metal cathode, since roughness or powder formation at metal cathodes, e.g. at a copper plate, is conditional upon depletion of the depositing ions near the surface (limiting current condition).

In situ measurement with holographic interferometry

It is desired to measure in situ the refractive index profile corresponding to the concentration profile of the ionic species formed at the lithium metal cathode. This in situ measurement technique is an important tool in the understanding and optimized design of "electrochemical processing for tailored materials". The present work thus focuses on the ionic mass transfer rate of Li^+ ions at the active Li metal cathode, which is associated with the transient natural convection at relatively high current density. The soundness of the present measurement technique has been demonstrated in our previous work [10], in which the concentration and velocity profiles associated with transient natural convection in Cu deposition from an aqueous $CuSO_4$ electrolyte system were quantitatively measured. The similarity between the present work and the earlier work on aqueous Cu deposition is based on the boundary layer character which both deposition processes have in common.

Experimental

Electrolytic cell

Having a high dielectric constant and low viscosity, propylene carbonate (PC) is known as a good candidate electrolyte for lithium secondary batteries. In this study, PC containing a predetermined concentration of 0.5 M $LiClO_4$ was used as received from Kishida Chemical. According to their analysis, the initial water content of the electrolyte solution was less than 30 ppm. Lithium foil of 200 μm thickness (Honjo Metal) was used as the working electrode. The counter electrode similarly was a 200-μm thick lithium foil and a quasi-reference electrode of 100-μm diameter Pt wire was used.

Figure 1 shows a schematic diagram of the electrolytic cell. The working and counter electrodes were vertically installed in a spectroscopic cell (10 mm×10 mm×40 mm high) of effective electrode area 15×6 mm^2. The electrode surfaces were placed face-to-face, separated by a 2-mm thick electrolyte layer. The Pt wire reference electrode was placed in the center of the electrolyte layer. In order to keep the lithium metal foil surface smooth, the foil was held on the flat surface of a glass plate by a Teflon spacer. This Teflon spacer also served to keep the two electrodes at the bottom of the cell parallel. Moreover, a glass capillary tube was inserted in the center of this spacer. It served to fix the focal plane at the center of the optical path, as mentioned later.

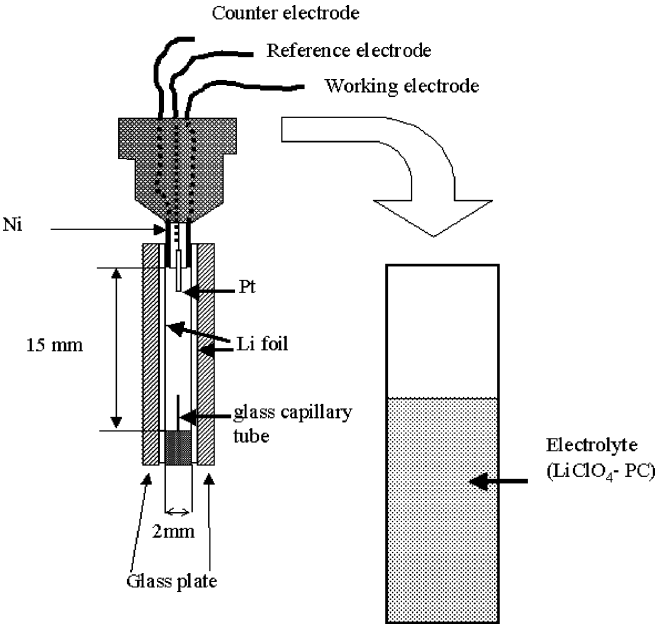

Fig. 1 Schematic diagram of the electrolytic cell

By filling the electrolytic cell made of optical glass, the two lithium foil electrodes were immersed in electrolyte and the cell was sealed by a Parafilm (American National Can) layer. This assembly always took place in a glove box filled with high-purity Ar gas, which was continuously circulated through molecular sieve 4A 1/16 (Nacalai Tesque) to remove water contaminant. Without continuous purification of the Ar gas stream by molecular sieve, the surface of the lithium foil became noticeably damaged very rapidly.

Holographic interferometry

Since Ibl and Muller's pioneering work [11], interferometry has been widely applied to study ionic mass transfer associated with natural convection induced by an electrochemical reaction. The optical arrangement used for the holographic interferometry is shown in Fig. 2 [12]. The light source was a 6 mW He-Ne laser (638.9 nm wavelength), which was split into objective and reference beams by a beam splitter (B). The reference beam was reflected by mirrors (M3, M4), expanded by a microscopic lens (E2), and projected onto a holographic film plate (Kodak high-speed holographic film SO-253). The objective beam was reflected by a mirror (M1), expanded by a microscopic lens (E1), and collimated by a lens (LE1). After the objective beam passed through the electrolytic cell, it was converged by a lens (LE2) in order to magnify the image on the holographic film plate. The objective beam flux was reflected by a mirror (M2) and superimposed on the holographic plate irradiated by the reference beam.

The holographic film plate was processed and fixed in the film holder (H) containing water. After development, the plate was moved in order to generate a horizontal interference fringe pattern. With the reference beam exposed onto the hologram plate, the wavefront of the objective beam passing through the electrolytic cell was reconstructed. The interference fringe pattern was observed with a charge coupled device (CCD) camera and stored on VHS video. The transient variation of the interference fringe pattern was recorded at various current densities.

The refractive index difference caused by concentration changes introduces an optical path length difference between the objective and reference beams. Thus, holographic interferometry may be used to determine concentration profiles. The average concentration along the optical path in the electrolytic cell can be measured

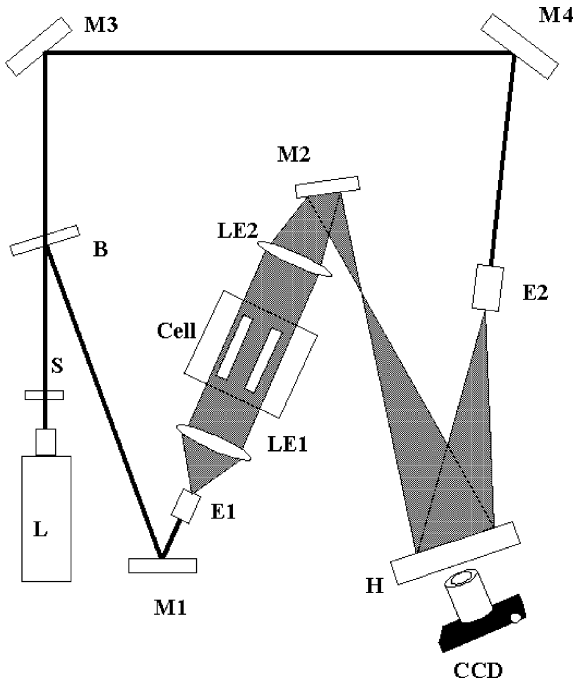

Fig. 2 Optical arrangement of the holographic interferometry

directly from the interference fringe shifts. When Z is the geometrical path length of the electrolytic cell and Δn the refractive index difference between the electrolyte at the cathode surface and the bulk electrolyte, the phase change of the objective beam or the number of interference fringes shifted, N, is given by:

$$N\lambda = Z(\Delta n) \tag{1}$$

The optical path length is the primary determinant of the resolution power of the interferometer. It is also a crucial parameter in the interpretation of the interferogram, since the refractive index gradient present in a very long transverse distance may also introduce a serious error due to an optical deflection effect [12, 13, 14, 15, 16, 17, 18, 19]. Moreover, it is essential to maintain the working electrode surface parallel to the objective beam. As mentioned above, the glass capillary tube at the center of the cell served to focus the beam. The image of the working electrode surface was kept at the farthest location from the cathode surface in order to ensure the objective beam was parallel [17]. The spatial resolution power of the present optical arrangement is of the order of 10 μm.

Refractive index

The relationship between the refractive index and the concentrations of solute species must be known in order to interpret the interference fringe shift. The effects of $LiClO_4$ and H_2O concentration on the refractive index of the PC electrolyte were measured with Abbe's refractometer (type PRA-B, Hitachi). The H_2O content of the electrolyte was determined by coulometric Karl-Fisher titration (AQ-200, Hiranuma). It was found that the H_2O concentration in PC could be maintained at less than 200 ppm or 1.4×10^{-2} M throughout the present experiments. Moreover, the measured dependence of $LiClO_4$ and H_2O concentrations on the refractive index of the PC electrolyte was of the order of 8×10^{-3} $M^{-1}$and -8×10^{-3} M^{-1}, respectively [20]. As the first step in this research, we focus on the transient concentration boundary layer thickness. Since the optical measurement is designed to be carried out at high current density, the concentration of H_2O is neglected in a first-order approximation. As described separately, the effect of H_2O concentration becomes apparent only at lower current density.

Results

A constant current step of 5–10 mA/cm^2 was applied to the Li cathode vertically immersed in the PC electrolyte containing 0.5 M $LiClO_4$. The electrode potential quickly shifted in the negative direction at the beginning of the electrolysis, and reached the steady potential of the lithium reduction reaction through the minimum potential. Figure 3 demonstrates the refractive index profile formed near the lithium cathode. At the beginning of electrodeposition, the interference fringe pattern is perpendicular to the vertical plane of the cathode. As time passes, the interference fringe starts to shift downward. When the current density is very high, the image of the cathode surface starts to recede. This is caused by optical beam deflection in a steep refractive index gradient, as pointed out above and analyzed by several authors [14, 17, 18, 19]. Moreover, the image of the cathode surface becomes less sharp with the progress of the electrodeposition. This may be due to the roughness developing at the active Li metal cathode surface during the electrodeposition through the SEI (solid electrolyte interface) layer.

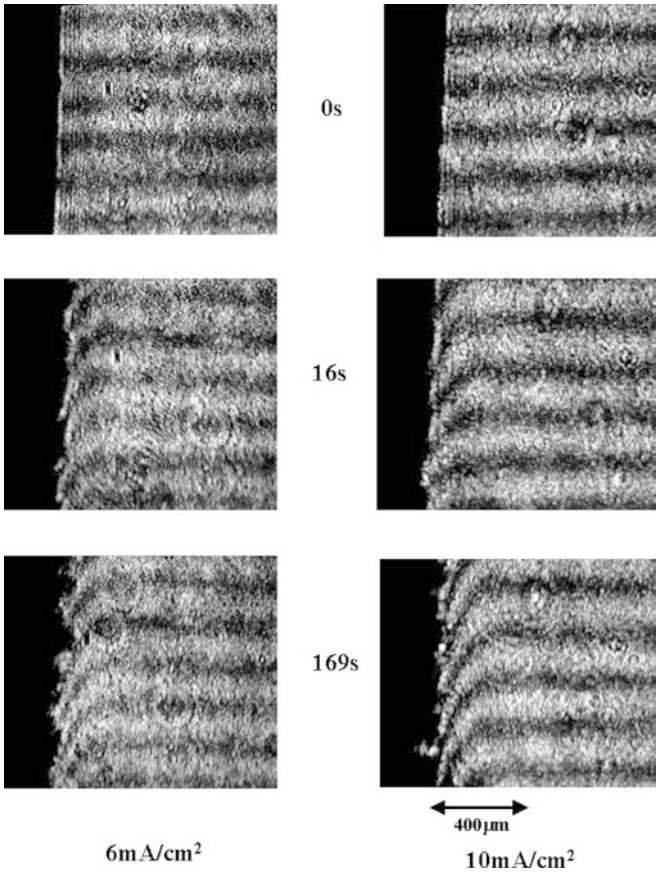

Fig. 3 Transient variation of the holographic interference fringe

The optical path length is rather longer in the present system. The effect of optical beam deflection may not be negligible at a high current density, when the laser beam proceeds perpendicularly to the refractive index gradient or the laser wave front is parallel to the refractive index gradient. Because of this steep refractive index gradient, the interference fringe shift number at the Li metal cathode surface could not be measured. However, the laser beam is straight in the uniform refractive index field outside of the concentration boundary layer. Therefore, once the original location of the cathode surface is recorded in a hologram before current passage, it is possible to measure the transient variation of the concentration boundary layer thickness, δ, with the progress of electrodeposition. δ is then defined as the distance between the locations at which the horizontal interference fringe starts to shift and the original location of the cathode in the hologram before current passage, as shown in Fig. 3.

As Fig. 3 shows, δ grows with time once the interference fringe starts to shift, until it reaches a virtual steady-state value around 150 s. The higher the current density, the thinner the boundary layer thickness in the steady state. This is characteristic for the development of transient natural convection due to electrodeposition at a vertical plane cathode in an unstirred electrolyte. In this respect, the ionic mass transfer rate of lithium ions interacts with the transient natural convection similarly as in the case of an aqueous electrolyte solution. However, several features, which are specific for lithium deposition, were observed. During careful observation of the video image, an upward schliere or a piece of passivation film (probably consisting of the SEI) was clearly visible along the vertical cathode, and a downward schliere was visible along an anode surface. It was sometimes observed that part of a dendrite arm broke off and was carried away by convection. In a lithium metal secondary battery, the existence of "dead lithium" (i.e. pieces of lithium metal disconnected from the negative electrode) is one of the most serious problems [21]. The velocity profile of the electrolyte was measured by monitoring the movement of a schliere or a piece of SEI to determine the maximum velocity, u_m.

As the electrodeposition time increases, the cathode surface becomes increasingly rough. An independent experiment was carried out to carefully observe the Li metal cathode surface using confocal laser microscopy [22]. Lithium was electrodeposited on the edge of a 180-μm thick film of Li metal. Some dendrite precursors of 10 μm size were noticed after passage of 0.1 C/cm^2. These precursors develop later to massive dendrite arms as the electrodeposition proceeds further. Dendrite arms 100 μm high above the Li metal cathode substrate were observed in the interferogram as well as in the real image. They grow in a concentration boundary layer whose thickness is 300 μm. The interference fringe pattern was fluctuating where it coincided with a dendrite arm.

Discussion

The characteristic features of transient natural convection developing along a vertical plane cathode are first described using, as an example, natural convection during Cu electrodeposition in aqueous $CuSO_4$ solution. Later the experimental data in a $LiClO_4$–PC electrolyte system are compared to this. The choice of aqueous $CuSO_4$ solution is based on the classical works by Wagner [1], Brenner [2], Ibl and Muller [11], and Wilke et al. [23], who used the electrodeposition of copper in aqueous $CuSO_4$ solution to demonstrate that the ionic mass transfer rate associated with natural convection induced by electrodeposition at a vertical plane electrode in a stagnant electrolyte can be predicted by the boundary layer theory [10, 12]. Comparison with their works may provide us with insight into the ionic mass transfer rate in non-aqueous electrolytes and help pinpoint similarities as well as differences.

Transient natural convection in aqueous electrolyte solution

When electrodeposition of Cu^{2+} ions takes place at constant current density on a vertical plate cathode immersed in a quiescent aqueous $CuSO_4$ solution, Cu^{2+} ions are transferred by a diffusion and migration mechanism [24, 25]. In the dilute solution theory usually applied, the migration effect is taken into account by the transference number of the Cu^{2+} ions and the diffusion of $CuSO_4$ is defined in terms of ion diffusivities. As time progresses, a density difference between the electrolyte near the cathode and that in the bulk develops, which induces a transient natural convection along the vertical plane cathode. The concentration difference between the electrolyte near the cathode surface and the bulk electrolyte, Θ_w ($=\Delta c = c^S - c^*$), as well as the concentration boundary layer thickness, δ, can be measured by laser interferometry, as discussed in earlier papers [26] and detailed above. Moreover, the maximum velocity of upward natural convection, u_m was successfully measured by the tracer technique with colophonium particles 10 μm in diameter [27]. The effect of electrode height, x, and current density, i, on the parameters Θ_w, δ, and u_m has been demonstrated to agree with boundary layer theory, as developed below. Thus, the data measured for Θ_w, δ, and u_m in transient natural convection may be normalized with respect to their values in the virtually steady state. It is our objective to compare these normalized experimental values with calculated, i.e. predicted, values.

Model equations and solution

The following assumptions have been made to develop and solve a set of model equations describing the ionic

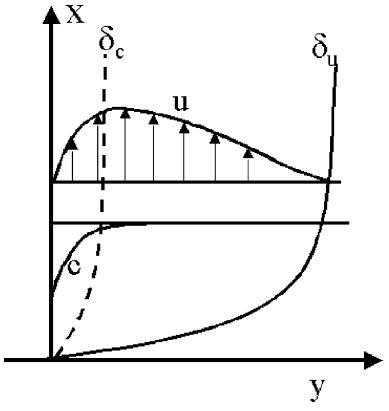

Fig. 4 Schematic illustration of natural convection along a vertical electrode

mass transfer rates as well as the momentum transfer rate.

1. A two-dimensional rectangular coordinate system is introduced with a doubly semi-infinite field representing the electrolyte.
2. The current density distribution along the vertical cathode is uniform.
3. The electrolyte flow generated by the cathode is laminar.
4. All transport properties are constant and uniform across the (x, y) field.

The model is schematically illustrated in Fig. 4.

The conservation equation for the reacting species (Cu^{2+} or Li^{+}) ion is described by:

$$\frac{\partial c}{\partial t} + u\frac{\partial c}{\partial x} + v\frac{\partial c}{\partial y} = D\frac{\partial^2 c}{\partial y^2} \tag{2}$$

The momentum balance equations are as follows:

$$\frac{\partial u}{\partial t} + u\frac{\partial u}{\partial x} + v\frac{\partial u}{\partial y} = v\left(\frac{\partial^2 u}{\partial x^2} + \frac{\partial^2 u}{\partial y^2}\right) + g\alpha(c - c*) \tag{3}$$

$$\frac{\partial v}{\partial t} + u\frac{\partial v}{\partial x} + v\frac{\partial v}{\partial y} = v\left(\frac{\partial^2 v}{\partial x^2} + \frac{\partial^2 v}{\partial y^2}\right) \tag{4}$$

Moreover, the continuity equation is:

$$\frac{\partial u}{\partial x} + \frac{\partial v}{\partial y} = 0 \tag{5}$$

The initial conditions may be expressed as:

$$u = v = 0,\ c = c* \text{ at } t = 0 \quad x > 0,\ y > 0 \tag{6}$$

The boundary conditions are:

$$u = v = 0,\ c = c* \quad \text{at } x = 0,\ y > 0 \tag{7}$$

$$u = v = 0,\ j = \frac{i(1 - *t_1)}{zF} = -D\left(\frac{\partial c}{\partial y}\right)_{y=0} \quad \text{at } y = 0 \tag{8}$$

$$u = 0, \quad c = c* \quad \text{at } y = \delta_u \tag{9}$$

The number of mesh along the x coordinate is set evenly to 100. The mesh along the y coordinate is assigned unevenly to 100 in a manner of geometric progression. The minimum size of mesh in the y direction is 1 μm and the maximum is 140 μm. The concentration boundary layer thickness was defined as the distance from the cathode surface where the concentration difference Θ $(= c^* - c)$ is 5% of the surface concentration difference Θ_w $(= c^* - c(y = 0) = c^* - c^S)$.

The calculated transient values of Θ_w, δ, and u_m are normalized with respective to the values of Θ_w^∞, δ^∞, and u_m^∞ at steady state. These normalized values are plotted against the normalized time T, as defined below. The calculated values are reasonably close to the measured ones, as demonstrated in Figs. 5a, 5b, and 6. All data were taken from measurements in 0.6 M aqueous $CuSO_4$ solution reported previously [10, 26, 27]. Θ_w/Θ_w^∞ increases linearly with the square root of the non-dimensional time T and reaches a practically steady value around 100–200 s at any given current density (Fig. 5a). δ/δ^∞ also increases with $T^{1/2}$, irrespective of the current density (Fig. 5b). Its transient behavior is primarily determined by the diffusion of $CuSO_4$ in the initial stage. On the other hand, the transient behavior of u_m/u_m^∞ shows apparently a larger inertial effect for the natural convection (Fig. 6). By the accumulated electrolyte density difference between the cathode surface and bulk electrolyte, natural convection is gradually induced.

Gebhart [28] originally analyzed the development of transient natural convection along a vertical plane heater with the similarity principle in which a similar temperature and velocity profile at various locations and time were assumed. The same technique was applied to an electrochemical system by the present authors [10], since the mathematical formulation is similar. It predicts that the transient diffusion equation can be applicable until the non-dimensional time, T, reaches 0.1. T is defined as:

$$T = Dt \Big/ \left(\overline{\delta}\right)^2 \tag{10}$$

where δ is a concentration boundary layer thickness averaged over a working electrode height in a steady state. It is the reason why the transient behavior of these non-dimensional parameters shows almost no dependence on the current density.

The Cu^{2+} ion concentration depletion and the upward velocity profile adjacent to the cathode surface start after a certain time, which depends on the height of the cell. The mass transfer rate couples simultaneously with the momentum transfer rate. When T exceeds 0.4, the transient natural convection reaches a virtual steady state. When the transient natural convection develops slowly, the ionic mass transfer rate of the metal ion may exceed a certain value and then relax slightly by the onset of natural convection. In the transition period between the transient diffusion and the steady-state natural convection, a so-called "overshooting" phe-

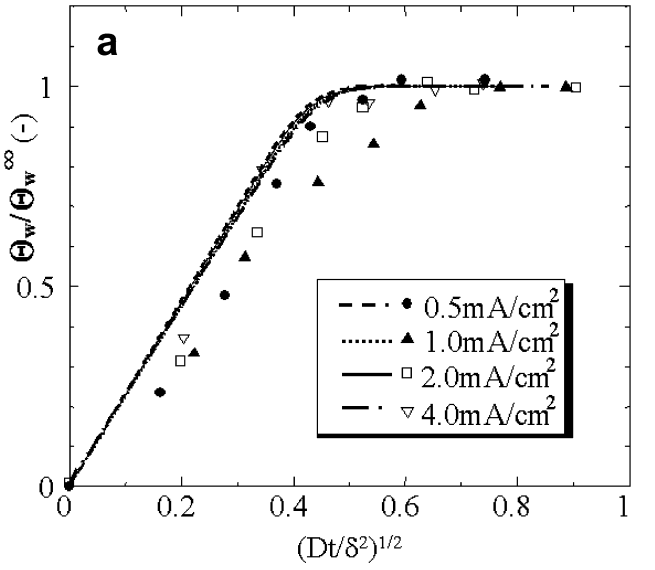

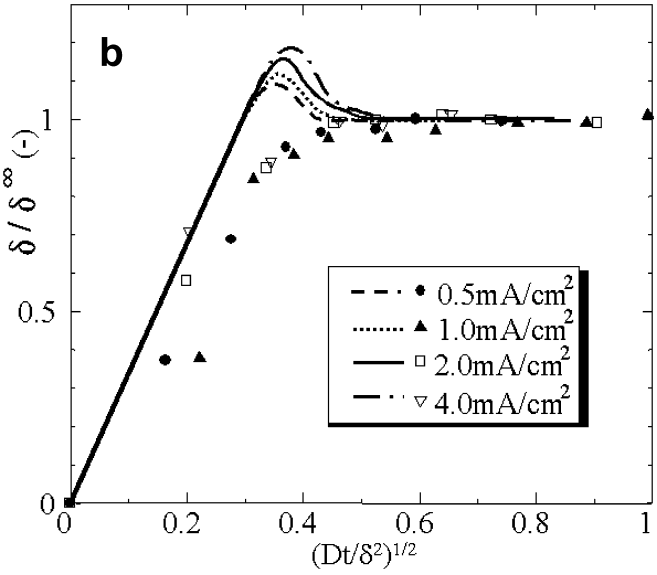

Fig. 5 (**a**) Time variation of concentration of Cu^{2+} ions at a copper cathode surface in 0.6 M $CuSO_4$ solution. (**b**) Development of concentration boundary layer thickness in 0.6 M $CuSO_4$ solution

nomenon appears in the calculation. It has been experimentally and numerically confirmed by Goldstein and Eckert [29] in their heat transfer experiments, but not in this mass transfer experiment (see Fig. 5b).

In the steady state, the concentration profiles of Cu^{2+} ions and the maximum velocity of upward natural convection, u_m, under the presumption of uniform current density distribution was correlated with the Rayleigh number, Ra_x*:

$$Sh_x = 0.628(Ra_x*)^{1/5} \quad \left(10^8 < Ra_x* < 10^{13}\right) \tag{11}$$

$$u_m x \Big/ D_1 = 1.05(Ra_x*)^{2/5} \quad \left(10^8 < Ra_x* < 10^{13}\right) \tag{12}$$

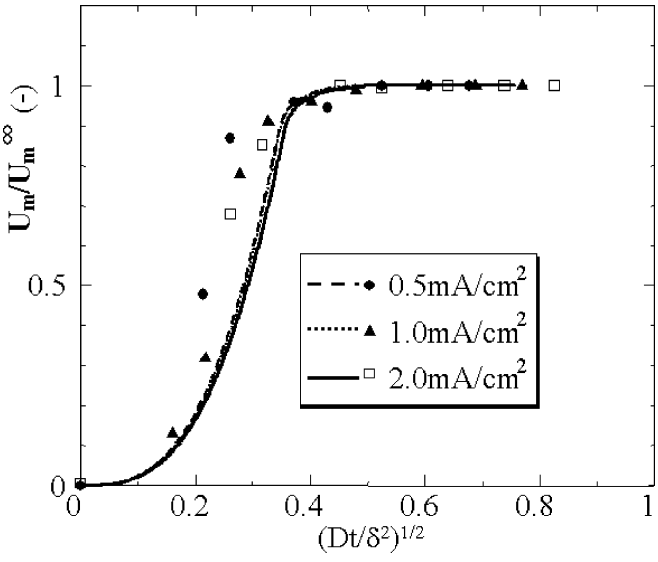

Fig. 6 Time variation of velocity near copper cathode surface in 0.6 M $CuSO_4$ solution

Experimental steady-state data show that the higher the current density, the thinner the concentration boundary layer thickness [12, 17, 30]. Also, the larger the surface concentration difference, the higher the maximum velocity. A reasonable agreement is observed in steady-state experiments as long as the assumptions that the electrode surface is geometrically flat and that the working electrode is installed in a semi-infinitely large electrolyte solution are valid, so that the effect of the counter electrode can be neglected. Since the agreement between the measured and the calculated values is satisfactory even in the transient period, it may be concluded that the transient natural convection behavior associated with constant current Cu electrodeposition in aqueous $CuSO_4$ solution is described to within 20% by the above approximate analysis. More rigorous FEM calculation is now under progress in a two-dimensional field of an electrolytic cell enclosed with two vertical plates of cathode and anode.

Transient natural convection in a $LiClO_4$–PC electrolyte

Figure 7 shows the time variation of the concentration boundary layer thickness, δ/δ^∞, with the square root of T at various current densities. δ/δ^∞ grows linearly with $T^{1/2}$ at any current density, once the interference fringe starts to shift. It reaches a virtual steady state around 100–200 s, although the measured data are more scattered than the case in aqueous solution. The solid lines correspond to the calculated concentration boundary layer thickness for various current densities. Physical properties adopted in this calculation are listed in Table 1 [31]. Good agreement is again observed between the calculated and measured boundary layer thickness, as in the case of the aqueous solution. Again, similarly as in aqueous solution, an "overshooting" of the diffu-

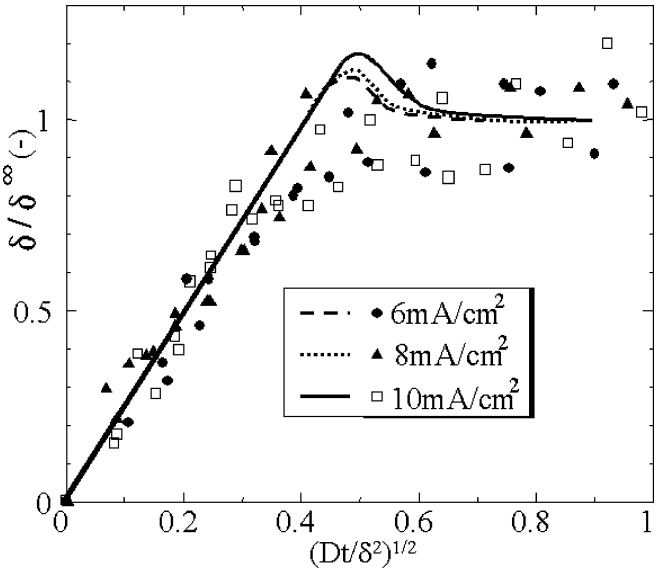

Fig. 7 Development of concentration boundary layer thickness in 0.5 M $LiClO_4$–PC electrolyte solution

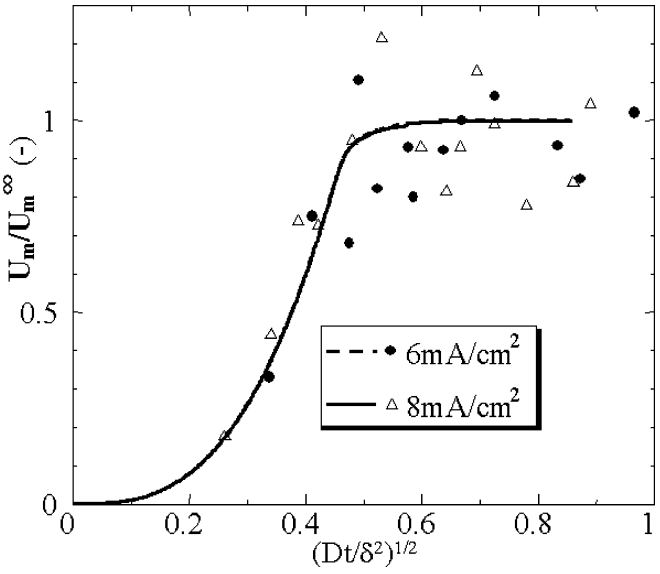

Fig. 8 Time variation of velocity near lithium cathode surface in 0.5 M $LiClO_4$–PC electrolyte solution

Table 1 Physical properties of 0.6 M aqueous $CuSO_4$ solution and 0.5 M $LiClO_4$–PC electrolyte solution

Composition[a]	0.6 M $CuSO_4$	0.5 M $LiClO_4$–PC
D_1 (10^{-6} cm^2 s^{-1})	4.4	2.9
ν (10^{-2} cm^2 s^{-1})	1.1	4.0
α (10^2 cm^3 mol^{-1})	1.55	0.72
$^*t_1$	0.29	0.44

[a] D_1, diffusivity; ν, viscosity; α, densification coefficient; $^*t_1$, transference number

sion layer thickness, predicted by the model, is not observed.

The calculated transient behavior of the maximal velocity of natural convection depicted by a solid line is compared with the measured values in Fig. 8. As easily imagined, it is more difficult to determine the maximum velocity of natural convection. The measured nondimensional maximal velocity u_m/u_m^∞ is thus scattered in a virtually steady-state condition. Nevertheless, the present model reasonably explains the measured transient behavior of natural convection and appears to do so better than in the aqueous electrolyte case.

A fairly good agreement is illustrated between the calculated and observed values in the transition to steady state. Small discrepancies are noticed in the absolute value of the steady-state concentration boundary layer thickness as well as the current density dependence of the mass transfer rate with natural convection. They are described separately (Ota M, et al., in preparation). The assumption in the simulation of a doubly semi-infinite diffusion field must be examined, as well as the validity of the assumption of surface flatness. The uncertainty of the physical properties may also relate to the discrepancy.

Overall, the results indicate that the ionic mass transfer rate of Li^+ ions in transient natural convection develops similarly as in the case of an aqueous electrolyte solution.

Conclusions

Li metal was electrodeposited from a $LiClO_4$–PC electrolyte on a vertical Li metal cathode. Holographic interferometry was used to study the ionic mass transfer process in the presence of natural convection in a nonaqueous electrolyte solution. The transient behavior of the interference fringes was successfully measured and correlated with lithium metal electrodeposition on the lithium cathode. The development of the concentration boundary layer thickness and the maximal velocity of electrolyte flow are explained with reasonable accuracy ($\pm 20\%$) by the development of a boundary layer with assumption of concentration and velocity profile similarity at all times during the transition. With the progress of electrodeposition, Li metal dendrites grow on the Li metal cathode. The surface roughness caused by electrodeposition appears to interfere and cause a large scatter in the measured steady-state value of the concentration boundary layer thickness of natural convection.

Acknowledgements The authors would like to thank Drs. F. McLarnon, Y. Ito, T. Ozuku, K. Kanamura, and Y. Uchimoto for their encouragement and suggestions. Part of this work was carried out under the financial aid given to the authors by the Ministry of Education, Science and Technology (project no. 11450285), ISAS, and NASDA, for which the authors are grateful.

References

1. Wagner C (1949) Trans Electrochem Soc 95:161
2. Brenner A (1940) Proc Am Electroplat Soc 95

3. Peled E (1979) J Electrochem Soc 126:2047
4. Peled E, Golodnitsky D, Ardel G, Eshkenazy V (1995) Electrochim Acta 40:2197
5. Aurbach D, Zaban A (1993) J Electroanal Chem 384:155
6. Aurbach D, Zaban A (1994) J Electroanal Chem 367:15
7. Takehara Z (1997) J Power Sources 68:82
8. Brissot C, et al. (1998) Electrochim Acta 43:1569
9. Brissot C, Rosso M, Chazalviel JN, Lascaud S (1999) J Electrochem Soc 146:4393
10. Fukunaka Y, Kondo Y (1981) Electrochim Acta 26:1357
11. Ibl N, Muller RH (1985) Z Electrochem 59:671
12. Denpo K, Okumura T, Fukunaka Y, Kondo Y (1985) J Electrochem Soc 132:1145
13. Hauf W, Grigull U (1970) Advances in heat transfer, vol 6. Academic Press, New York, p 133
14. Muller RH (1973) Advances in electrochemistry and electrochemical engineering, vol 9. Wiley, New York, p 281
15. Mayingr F, Panknin W (1978) Venfahrenstechmic 12:582
16. McLarnon FR, Muller RH, Tobias CW (1975) J Opt Soc Am 65:1011
17. Fukunaka Y, Denpo K, Iwata M, Maruoka K, Kondo Y (1983) J Electrochem Soc 130:2492
18. McLarnon FR, Muller RH, Tobias CW (1975) J Electrochem Soc 122:59
19. Beach KW, Muller RH, Tobias CW (1973) J Opt Soc Am 63:559
20. M. Ota (2002) MS thesis. Kyoto University, Kyoto, Japan
21. Yamaki J, et al. (1998) J Power Sources 74:219
22. Izuo S (1998) MS thesis Kyoto University, Kyoto, Japan
23. Wilke CR, Eisenberg M, Tobias CW (1953) J Electrochem Soc 100:513
24. Newman J (1973) Electrochemical systems, Prentice-Hall, Englewood Cliffs, NJ
25. Selman JR, Newman J (1971) J Electrochem Soc 118:1070
26. Urano H, Kondo Y (1978) Denki Kagaku 46:330
27. Tsukada H, Kondo Y (1978) Denki Kagaku 46:337
28. Gebhart B (1961) J Heat Transfer 83:61
29. Goldstein RJ, Eckert ERG (1960) Int J Heat Mass Transfer 1:208
30. Denpo K (1983) PhD Dissertation. Kyoto University, Kyoto Japan
31. Videa M, Xu W, Geil B, Marzke R, Angell CA (2001) J Electrochem Soc 148:A1352